AC–DC LED Driver With an Additional Active Rectifier and a Unidirectional Auxiliary Circuit for AC Power Ripple Isolation

Zhenyu Shan, *Member, IEEE*, Xiaomei Chen, Juri Jatskevich, *Fellow, IEEE*, and Chi K. Tse, *Fellow, IEEE*

***Abstract*—Single-phase ac light-emitting diode (LED) lamps require long-lifespan and high-efficiency ac–dc power converters for power factor correction (PFC) and current regulation. In such converters, the inherent double-line-frequency ripple power from the ac source is isolated from the load by large electrolytic capacitors (E-caps) or E-cap-less active circuits to improve reliability and lifespan. This paper presents an ac–dc LED driver with an additional active rectifier and a unidirectional auxiliary circuit for ripple power isolation. As compared with other similar designs, the proposed LED driver operates with reduced redundant power processing and a lower voltage on the storage capacitor, and the additional active circuits include fewer power components. The prototype with small polymer-hybrid capacitors and ceramic capacitors is separately tested in the experiment.**

***Index Terms*—AC–DC converters, auxiliary circuit, light-emitting diode (LED), LED driver, power factor correction (PFC).**

I. Introduction

LIGHT-EMITTING diode (LED) lamps are widely used in lighting systems and are expected to dominate the future lighting market [1]–[4]. Different from other lighting devices, such as incandescent bulbs and fluorescent tubes, LEDs are driven by dc current source, which is generally realized by switching-mode power converters [5]. For LED lamps powered by the utility grid, the LED driver achieves a typical power conversion from a single-phase ac source to dc loads.

The power flow in ac–dc LED drivers is illustrated in Fig. 1. At the input side, the power flow $p_{\rm in}(t)$ includes a constant power $P_{\rm in}$ and a double-line-frequency ripple power $p_r(t)$ when a unity power factor (PF) is achieved. At the output side, the voltage V_o is clamped and close to the forward voltage of the diode V_F, and the current I_o must be regulated. The resulting power flow P_o at the output port is constant. In traditional ac–dc converters, a large capacitor is directly connected to the output port to isolate the ripple power $p_r(t)$ from the load, as shown in Fig. 1. As presented in [6], the required minimum capacitance is determined by

$$C\Delta V = \frac{P_o}{2\pi f V_o} \tag{1}$$

where f is the line frequency and ΔV is the allowed voltage ripple on the output port. In LED applications, ΔV must be very small because LED devices have a small equivalent series resistance. A small voltage ripple may cause a substantial current ripple and flicker that should be avoided in most lighting systems [7]–[9]. To meet the requirement for storage, electrolytic capacitors (E-caps) are routinely used. However, the lifetime of general E-caps is in the order of thousands of hours, which is much shorter than LEDs' lifespan of up to 100 000 h [10]. Currently, although long-lifespan E-caps are available [11], [12], the cost is still prohibitive for most lighting systems, and such E-caps are bulky.

Several approaches to minimizing the capacitance for power ripple isolation have been reported [13]–[21]. A cascaded two-stage ac–dc LED driver with small capacitors has been proposed [13]. In such structure, the first-stage converter operates for power factor correction (PFC), and the second-stage converter for output current regulation. The intermediate voltage allows a relatively large ripple, which can significantly reduce the required capacitance for power ripple isolation. However, the efficiency of this LED driver may suffer from redundant

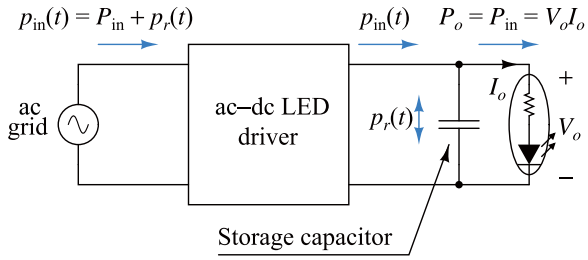

Fig. 1. Power flow of a conventional unity PF ac–dc LED driver with a large storage capacitor.

Manuscript received August 31, 2017; revised January 10, 2018; accepted February 18, 2018. Date of publication March 5, 2018; date of current version November 19, 2018. This work was supported in part by the National Natural Science Foundation of China under Grant 51477144 and Grant 51777002, in part by Beijing Natural Science Foundation under Grant 3184045, and in part by the Startup Scientific Research Foundation, North China University of Technology. Recommended for publication by Associate Editor L. Huber. *(Corresponding author: Zhenyu Shan.)*

Z. Shan and X. Chen are with the Department of Electrical Engineering, North China University of Technology, Beijing 100041, China (e-mail: zhenyus@ncut.edu.cn; 2017311010129@mail.ncut.edu.cn).

J. Jatskevich is with the Department of Electrical and Computer Engineering, University of British Columbia, Vancouver, BC V6T 1Z4, Canada (e-mail: jurij@ece.ubc.ca).

C. K. Tse is with the Department of Electronic and Information Engineering, Hong Kong Polytechnic University, Hong Kong (e-mail: encktse@polyu.edu.hk).

Color versions of one or more of the figures in this paper are available online at http://ieeexplore.ieee.org.

Digital Object Identifier 10.1109/TPEL.2018.2812223

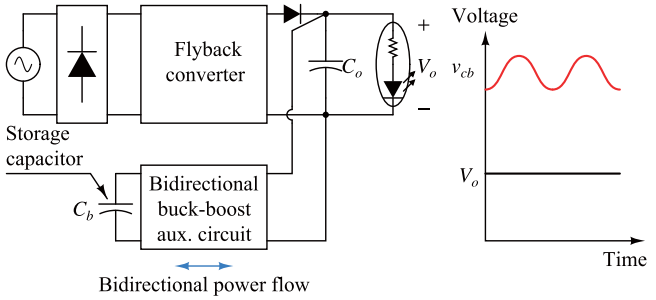

Fig. 2. AC–DC LED driver with a bidirectional buck–boost auxiliary circuit for double-line-frequency power ripple isolation [23].

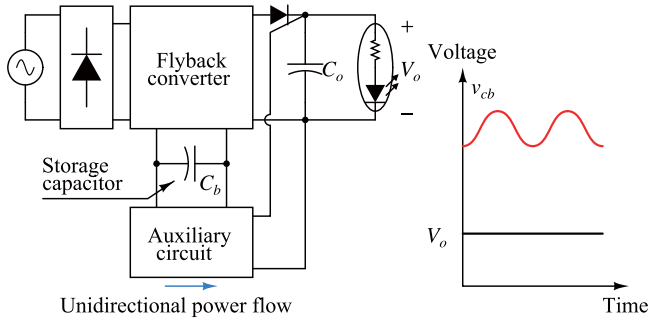

Fig. 3. LED driver based on a three-port flyback converter topology [27].

power processing [14]. Another approach to reducing the capacitance is to intentionally generate a high-order harmonic current at the input port of the LED driver [15], and two similar designs have also been presented [16]–[18]. The combination of the double-line-frequency power ripple and the high-order harmonic power can be buffered by much less energy storage. However, the input PF of these circuits is sacrificed. The aforementioned LED drivers feed a continuous current to the load, while a high-frequency pulsating-current LED driving method has also been proposed [19]. The duty cycle of the LED driving current is manipulated to make the average current constant over each switching cycle. At the end, the capacitance requirement is reduced due to larger allowable voltage ripples. Two similar approaches have also been proposed [20], [21]. However, as reported in [22], such LED drivers may lower the lighting efficiency of LED devices.

Apart from the approaches mentioned above, a single-stage configuration comprising a flyback converter operating in discontinuous current mode (DCM) for PFC and an auxiliary circuit for ripple power isolation has been developed [23]–[35]. This configuration achieves a unity PF and high efficiency while allowing a high-voltage ripple on the storage capacitor to reduce the capacitance requirement. In [23]–[25], a bidirectional buck–boost converter is employed to fully absorb the double-line-frequency power ripple at the output port of the LED driver, as shown in Fig. 2. The storage capacitor C_b is isolated from the LED loads by the auxiliary circuit, and therefore, allows higher dc voltage and larger voltage ripple. The power processed by the auxiliary circuit is $2P_o/\pi$. A similar topology based on the ripple port concept [6] has been proposed [26]. In [27], a series of LED drivers based on a three-port flyback converter were proposed. This concept is illustrated in Fig. 3, where a unidirectional auxiliary circuit is connected to the third port and the LED load. When the input power of the flyback converter is higher than the load power, the surplus part of the power flows to capacitor C_b through the third port and is then stored there; otherwise, the auxiliary circuit operates to make the power flow from capacitor C_b to the load. Comparing with the configuration shown in Fig. 2, the power processed by the auxiliary circuit is reduced by half of the ripple power, namely P_o/π. Other LED drivers derived with the similar concept were presented in [28]–[31]. In [32] and [33], a bidirectional full-bridge auxiliary circuit with capacitor C_a is connected in series to the output port of

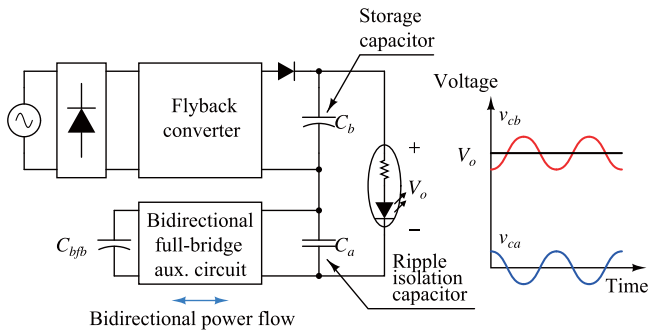

Fig. 4. AC–DC LED driver with a bidirectional full-bridge auxiliary circuit for ripple voltage cancellation, where the ripple power is partially processed by the bidirectional circuit [32].

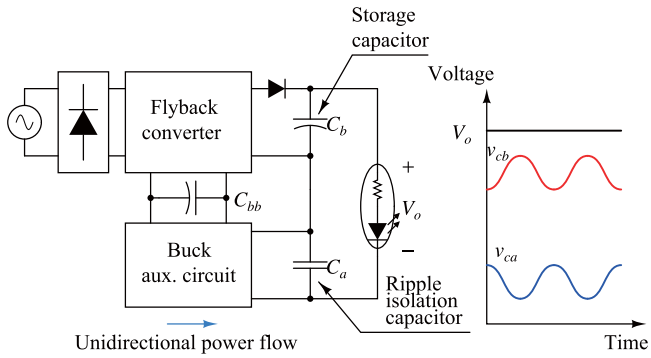

Fig. 5. AC–DC LED driver with a bidirectional buck–boost auxiliary circuit for ripple voltage cancellation, where the ripple power is partially processed by the bidirectional circuit [34].

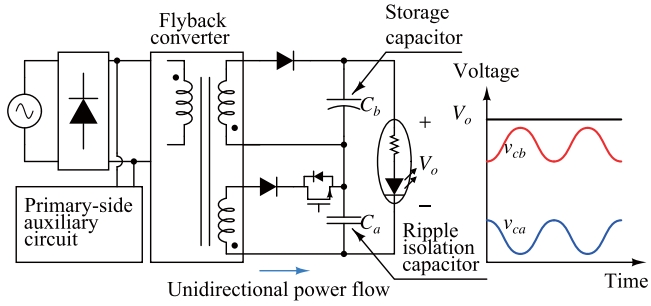

Fig. 6. LED driver with power ripple isolation using an energy channeling method [35].

TABLE I
CHARACTERISTICS OF THE PROPOSED LED DRIVER AND OTHER SIMILAR WORKS IN RIPPLE POWER DECOUPLING FOR AC–DC LED DRIVERS

LED driver	Ref.	Output power/voltage (P_o/V_o)	Power processed by the aux. circuit	No. of components in the aux. circuit				Storage capacitor				
				Switches	Diodes	Other (L, C)	Transformer windings	Operating voltage (V)	Capacitance (μF)	Voltage rated (V)	Type	Volume (cm^3)
Fig. 2	[23]	33.6 W/48 V	$0.637P_o$	2	0	2	0	85—136	2×10	250	Film cap.	18.3
	[24]	33.6 W/48 V		2	0	2	0	125—195	4.7	250	Film cap.	7.3
	[25]	20 W/33 V		2	0	2	0	230—250	3.7		Not reported	
Fig. 3	[27]	13.5 W/45 V	$0.318P_o$	2	1	1	1	120—210	3.3	400	Film cap.	18
	[28]	13.5 W/45 V	$0.318P_o$	2	2	1	1	120—250	3	630	Film cap.	24.3
	[29]	20 W/29.5 V	$> 0.318P_o$, $< 0.637P_o$	1	2	2	1	36—128	2×5.6	160	Film cap.	14.9
	[30]	19.6 W/28 V	$0.318P_o$	1	3	3	1	310—350	2×3.3	450	Film cap.	35.9
	[31]	16 W/80 V	$0.318P_o$	2	2	2	0	100—170	3×2.2	400	Film cap.	32.4
Fig. 4	[32]	100 W/150 V	$0.124P_o$	4	0	3	0	132—169	56	250	Film cap.	57.4
	[33]	100 W/150 V	$0.161P_o$	4	0	3	0	129—171	2×22	250	Film cap.	37.9
Fig. 5	[34]	35 W/50 V	$0.096P_o$	2	1	3	1	43—48	470	63	E-cap	5.12
Fig. 6	[35]	8.5 W/50 V	≈ 0	2	5	3	2	45—49	100 + 33	63	E-cap	1.18
Fig. 7 (proposed LED driver)		23 W/46 V	$0.065P_o$	2	2	2	0	37—43	3×100	50	Polymer E-cap	3.0
			$0.076P_o$	2	2	2	0	33—45	100 + 56	50	Polymer E-cap	2.0
			$0.109P_o$	2	2	2	0	26—45	100	50	Ceramic cap.	6.8

the flyback converter, as shown in Fig. 4. In this configuration, most of the double-line-frequency ripple power is directly absorbed by C_b, and the ripple voltage on it is compensated by the auxiliary circuit. The power processed by the auxiliary circuit is proportional to the amplitude of the ripple voltage and can be further reduced. In addition, the voltage stress of the auxiliary circuit is much lower than the LED voltage. An LED driver with the similar architecture (see Fig. 5) was proposed in [34]. In this LED driver, the output voltage of the auxiliary circuit is a bias dc voltage plus the ripple voltage. An LED driver with the energy channeling technology for voltage ripple cancellation was proposed in [35], as shown in Fig. 6. The power processed by the auxiliary circuit can be ideally reduced to almost zero. However, a primary-side auxiliary circuit that includes many components (not shown in detail) is needed.

A comprehensive comparison among these LED drivers and the proposed LED driver in this paper are shown in Table I. The auxiliary circuits proposed with the LED drivers in [23]–[25], [27]–[31] and shown in Figs. 2 and 3 consist of fewer components. The auxiliary circuits presented in [32]–[35] and shown in Figs. 4–6 process a lower power, which potentially achieve a lower energy loss for a given efficiency. This paper presents an LED driver with such two advantages, namely, a simple structure and low power processing of the auxiliary circuit.

The LED driver proposed in this paper consists of a flyback converter, an additional active rectifier, and a unidirectional auxiliary circuit, as shown in Fig. 7. As compared with the topologies in Figs. 2–6, the advantages of the proposed LED driver can be summarized as follows.

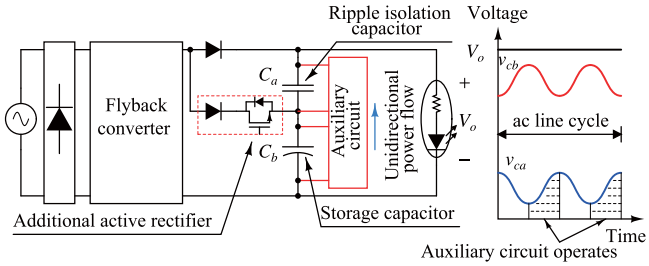

Fig. 7. Structure of the proposed ac–dc LED driver with an additional active rectifier and a unidirectional auxiliary circuit for power ripple isolation.

1) The auxiliary circuit with an additional active rectifier is implemented by only six components and does not need an additional winding in the flyback transformer. The LED driver proposed in this paper is comparable to that presented in [27]–[31] in terms of the number of components and the complexity. Furthermore, the output voltage of the auxiliary circuit is only a small part of the load voltage, which makes the power processing much lower than that in Figs. 2 and 3.
2) The output voltage of the auxiliary circuit is connected in series to the storage capacitor, which is similar to the design reported in [32]–[35] and illustrated in Figs. 4–6. However, it processes the unidirectional power flow as the input power of the LED driver is lower than its mean value. This potentially helps further reduce redundant power processing and the power loss. In addition, the proposed auxiliary circuit is composed of fewer

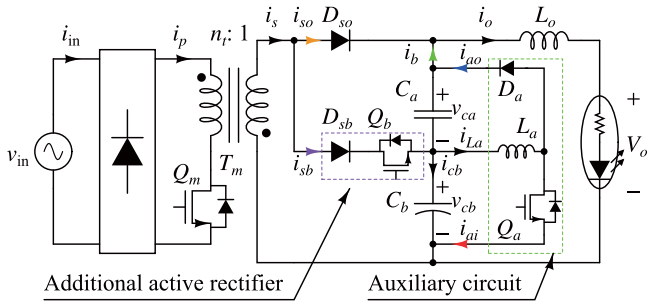

Fig. 8. Power stage of the proposed ac–dc LED driver.

components, comparing with these existing similar configurations.

3) The operating voltage of the storage capacitor is lower than the LED voltage, which helps reduce the size and cost. In most E-cap-less LED drivers, high-voltage film capacitors are used and occupy large space in [23], [24], and [27]–[33] (see Table I) and in [13] and [15]–[20]. Due to a low operating voltage of the proposed auxiliary circuit, an E-cap-less LED driver is realized with low-cost and low-volume ceramic capacitors in this paper.

II. Operating Principles of Proposed LED Driver

The proposed structure in Fig. 7 can be realized by the topology shown in Fig. 8. The flyback converter (main converter) consists of a diode bridge, a transformer T_m with the turns ratio of $n_t : 1$, and a switch Q_m. The additional active rectifier is composed of an active switch Q_b and a diode D_{sb}. Moreover, the auxiliary circuit is composed of a switch Q_a, an inductor L_a, and a diode D_a, which is similar to buck–boost circuits that are used for charge balancing in battery packs [36]. Here, capacitor C_b is used to buffer the input power ripple, and capacitor C_a is used for ripple isolation and filtering switching ripples of the auxiliary circuit and the flyback converter.

The key waveforms of the proposed LED driver (neglecting switching ripples) are illustrated in Fig. 9. The main converter is operating in DCM with a constant duty ratio applied to Q_m. The input current $i_{\rm in}(t)$ and voltage $v_{\rm in}(t)$ are inherently in phase. Thus, the input power $p_{\rm in}(t)$ has a double-line-frequency variation about the mean value $P_{\rm in}$, as shown in Fig. 9(a) and (b). When $p_{\rm in}(t) > P_{\rm in}$, the additional rectifier operates with power $P_{\rm in}$ flowing to the load and the surplus power $p_{\rm in}(t) - P_{\rm in}$ stored in capacitor C_b. When $p_{\rm in}(t) < P_{\rm in}$, the power $P_{\rm in} - p_{\rm in}(t)$ flows to the load from C_b, and the auxiliary circuit operates to charge C_a to compensate the voltage dip on C_b. The internal waveforms of the LED driver are shown in Fig. 9(c)–(e), including voltages on C_a and C_b [$v_{ca}(t)$ and $v_{cb}(t)$], the currents flowing to the load from the flyback converter and the storage capacitor [$i_{so}(t)$ and $i_b(t)$], and input/output currents of the auxiliary circuit [$i_{ai}(t)$ and $i_{ao}(t)$]. For ease of presentation, two time intervals, $[T/8, 3T/8]$ and $[3T/8, 5T/8]$ are, respectively, referred to as *charging cycle* and *discharging cycle*, since the storage capacitor C_b is, respectively, charging and discharging in these two periods of time.

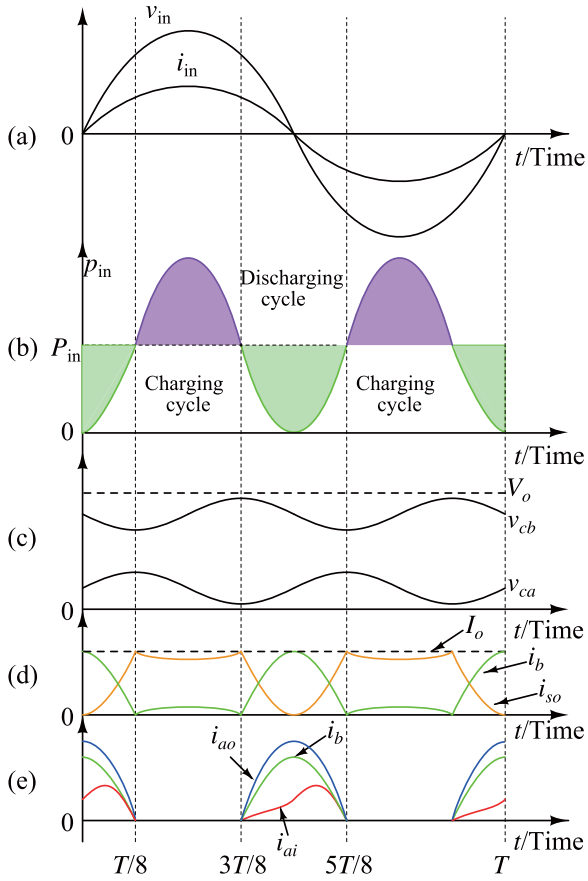

Fig. 9. Input and internal waveforms of the proposed LED driver in one cycle of the input voltage neglecting all switching ripples.

A. Operating Principles in Charging Cycles

During charging cycles [$p_{\rm in}(t) > P_{\rm in}$], the additional active rectifier operates to channel the input power and regulate the output current i_o, whereas the auxiliary circuit is not working. The secondary current $i_s(t)$ is divided into two parts, namely, $i_{so}(t)$ and $i_{sb}(t)$, as shown in Fig. 8. Current $i_{so}(t)$ flows to the load, which is ideally equal to load current I_o. Moreover, current $i_{sb}(t)$ is mainly charging the storage capacitor C_b, which causes $v_{cb}(t)$ to rise and $v_{ca}(t)$ to fall, and the sum of the two voltages is inherently equal to the LED voltage V_o, as shown in Fig. 9(c).

The detailed operating principles of the LED driver are illustrated in Fig. 10. The key waveforms in each switching period T_{sw_m} are shown in Fig. 10(a). In duration $[t_1, t_2]$, the main switch Q_m is on with duty cycle D_y, which makes current i_s zero and capacitors C_a and C_b discharged with voltage drops Δv_1 and Δv_2, as shown in Fig. 10(b). Switch Q_m is turned OFF at the instant of t_2, and current i_s becomes nonzero. In the duration $[t_2, t_3]$, current $i_{so} = i_s$ flows through diode D_{so} and charges the capacitors, leading to voltage increases Δv_3 and Δv_4, respectively, on C_a and C_b, as shown in Fig. 10(c). The switch Q_b turns ON at the instant of t_3. In the duration of $[t_3, t_4]$, current $i_{sb} = i_s$ flows through diode D_{sb}, resulting in voltage decrease Δv_5 on C_a and voltage increase Δv_6 on C_b, as shown in Fig. 10(d). For ease of presentation, the above-mentioned durations are defined as $d_{ro}T_{sw\_m}$ and $d_{rb}T_{sw\_m}$, respectively.

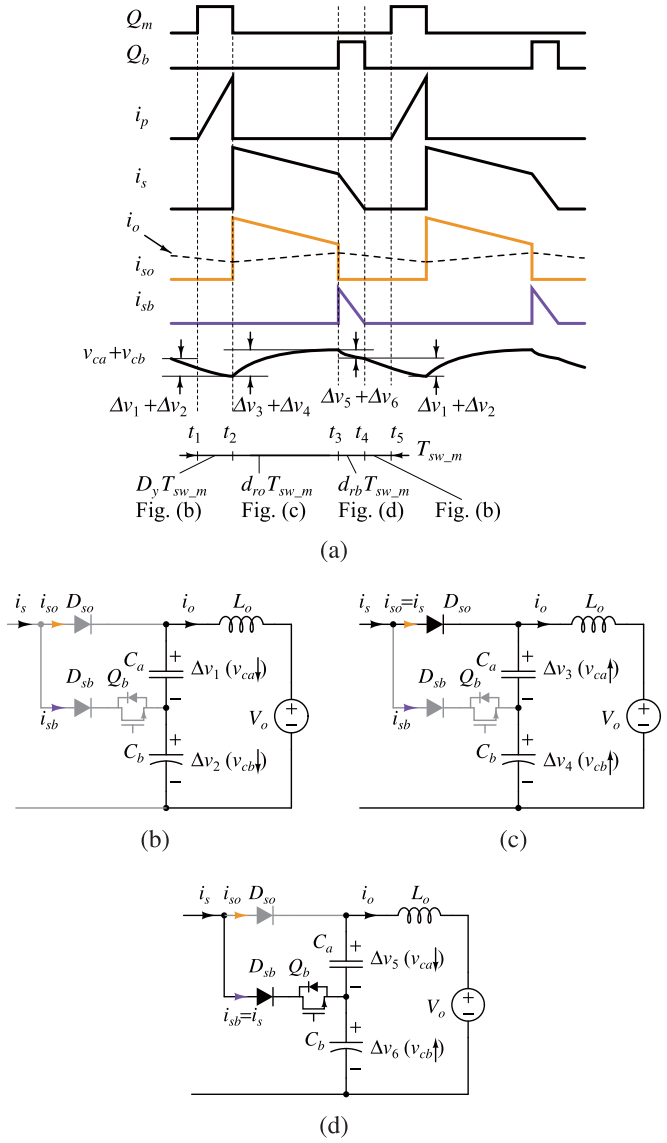

Fig. 10. Illustration of detailed operating principles of the LED driver in charging cycles. (a) Key waveforms in each switching period. (b)–(d) States of the secondary-side circuit (the LED load is represented by a voltage source V_o) in different durations.

The circuit state in duration $[t_4, t_5]$ is the same as that in $[t_1, t_2]$. The voltage changes on C_a and C_b in these two durations are considered together and denoted by Δv_1 and Δv_2. Over the entire switching period, the net change of the voltage $v_{ca} + v_{cb}$, i.e., the sum of Δv_1 to Δv_6, must be zero.

B. Operating Principle in Discharging Cycles

During discharging cycles, the auxiliary circuit operates to manage the voltage of C_a and regulate the load current, while the additional active rectifier is OFF. The current $i_s(t)$ is flowing to the load, and the power insufficiency, namely $P_{\text{in}} - p_{\text{in}}(t)$, is made up by the energy storage in capacitor C_b. With C_b discharging and voltage $v_{cb}(t)$ falling, the auxiliary circuit is charging C_a to make $v_{ca}(t)$ rise and the sum of them equal to V_o, as shown in Fig. 9.

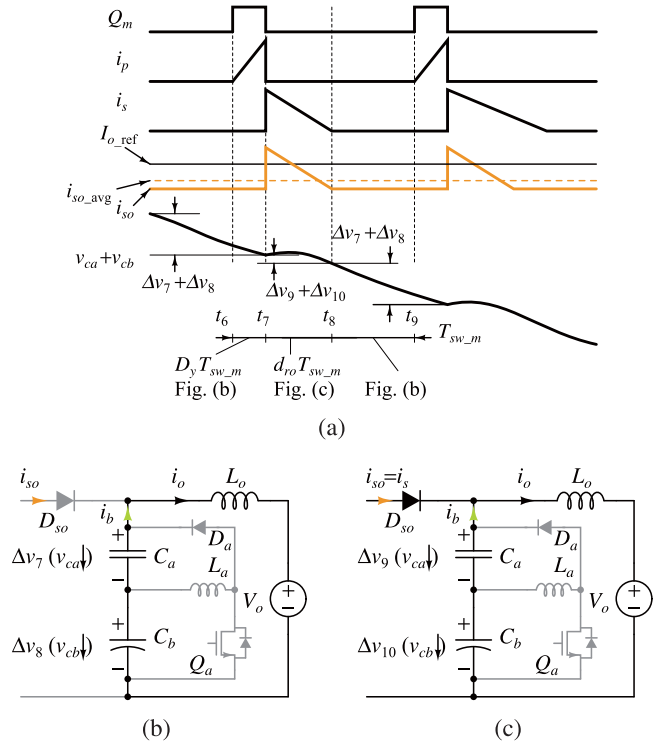

Fig. 11. Illustration of detailed operating principles of the LED driver in discharging cycles without the auxiliary circuit. (a) Key waveforms in each switching period. (b) and (c) States of the secondary-side circuit in different durations (the LED load is represented by a voltage source V_o).

Since the flyback converter and the auxiliary circuit can operate individually, the operating principles of these two parts are separately described and illustrated in Figs. 11 and 12. When only the flyback converter is considered, voltage changes on capacitors C_a and C_b during $[t_6, t_9]$ are denoted by Δv_7 to Δv_{10}, as shown in Fig. 11. Since the mean current from the flyback converter i_{so_avg} is lower than the load current, i.e., the sum of Δv_7 to Δv_{10} over one switching period is negative. Therefore, if the auxiliary circuit is not operating, voltage $v_{ca} + v_{cb}$ will fall, as shown in Fig. 11(a).

When the auxiliary circuit is simultaneously operating, the operating principle of the LED driver is illustrated by Fig. 12. In this situation, voltage $v_{ca} + v_{cb}$ will be fixed at V_o with a small ripple, as shown in Fig. 12(a). For ease of presentation, the actual current from the flyback converter is replaced by its mean value i_{so_avg}, as shown in Fig. 12(b)–(d). In duration $[t_{10}, t_{11}]$, switch Q_a is ON with duty cycle d_a, and the auxiliary circuit is sinking current i_{ai}, leading to the voltage change of Δv_{11} and Δv_{12}, respectively, on capacitors C_a and C_b, as shown in Fig. 12(a) and (b). In duration $[t_{11}, t_{12}]$, the auxiliary circuit is releasing current i_{ao} to charge capacitor C_a, resulting in the voltage change of Δv_{13} and Δv_{14}, respectively, on C_a and C_b, as shown in Fig. 12(a) and (c). During $[t_{12}, t_{13}]$, the voltage changes on C_a and C_b are, respectively, denoted by Δv_{15} and Δv_{16}, as shown in Fig. 12(a) and (d). When the output current is well regulated, the sum of Δv_{11} to Δv_{16} over one switching cycle will be equal to zero. It is noted that the switching period

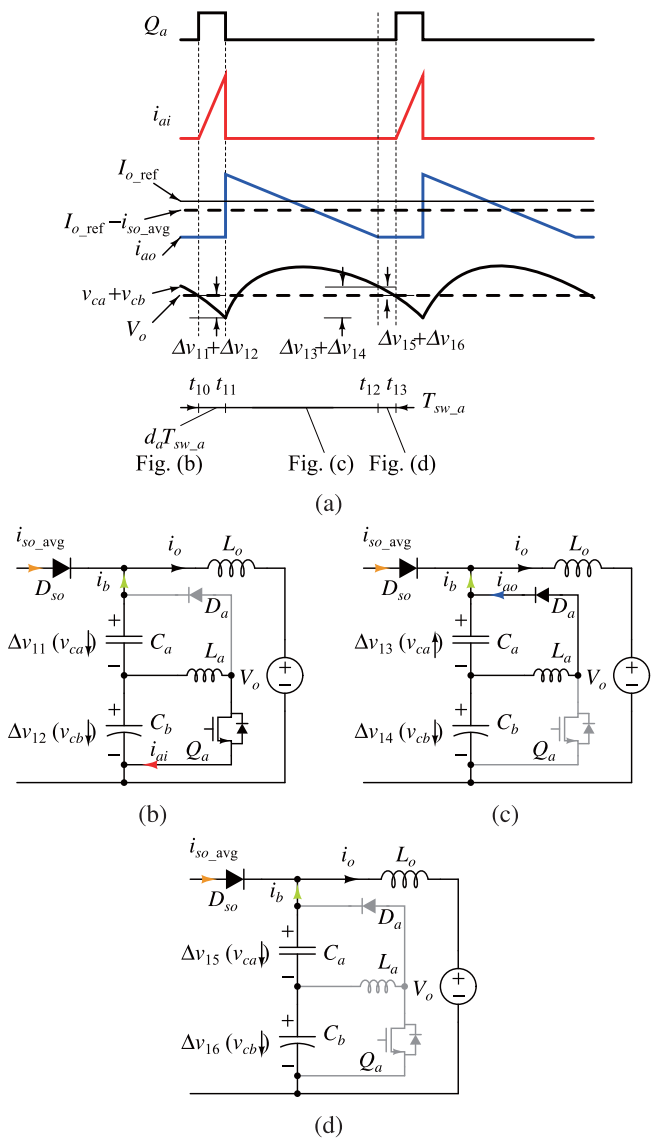

Fig. 12. Illustration of detailed operating principles of the LED driver in discharging cycles with the auxiliary circuit. (a) Key waveforms in each switching period. (b)–(d) States of the auxiliary circuit in different durations (the LED load is represented by a voltage source V_o and the pulsating current i_{so} from the flyback stage is superseded by its mean current i_{so_avg}).

of the auxiliary circuit may not be the same as that of the main converter, which is denoted by T_{sw_a}.

III. Circuit Analysis and Parameter Design

The required volume and voltage rating of capacitors can be derived from an analysis of the power flow of storage capacitors and the characteristics of the flyback converter circuit. Subsequently, the required inductor value of the auxiliary circuit can be obtained.

A. Power Flow of the Storage Capacitor

It is assumed that there are no power loss and high-frequency switching ripple in the LED driver that is operating with the unity PF. If the input voltage of the LED driver is

$$v_{\text{in}}(t) = V_m \sin \omega t \tag{2}$$

the instantaneous input power with double-line-frequency ripple will be

$$p_{\text{in}}(t) = P_o(1 - \cos 2\omega t). \tag{3}$$

Then, the ripple power $p_r(t)$ can be formulated as

$$p_r(t) = -P_o \cos 2\omega t. \tag{4}$$

Assuming that the ripple power is buffered by the capacitors and the energy storage there takes the form of

$$W_c(t) = \frac{1}{2}C_b v_{cb}(t)^2 + \frac{1}{2}C_a v_{ca}(t)^2 \tag{5}$$

we can get

$$\begin{aligned}\frac{dW_c(t)}{dt} &= C_b v_{cb}(t)\frac{dv_{cb}(t)}{dt} + C_a v_{ca}(t)\frac{dv_{ca}(t)}{dt} \\ &= -P_o \cos 2\omega t.\end{aligned} \tag{6}$$

Substituting $v_{ca}(t) = V_o - v_{cb}(t)$ into (6), the solution of the equation is derived as

$$\begin{aligned}v_{cb}(t) &= K_1 + \sqrt{K_2 - K_3 \sin 2\omega t}, K_1 = \frac{C_a}{C_a + C_b}V_o, \\ K_2 &= (V_{cb0} - K_1)^2, K_3 = \frac{V_o I_o}{(C_a + C_b)\omega}\end{aligned} \tag{7}$$

where V_{cb0} represents $v_{cb}(0)$, namely the initial value of $v_{cb}(t)$. Then, $i_{cb}(t)$ can be derived as

$$i_{cb}(t) = C_b\frac{dv_{cb}(t)}{dt} = \frac{-K_4 \cos 2\omega t}{\sqrt{K_2 - K_3 \sin 2\omega t}}, K_4 = \frac{C_b P_o}{C_a + C_b}. \tag{8}$$

When C_a is much smaller than C_b, $v_{cb}(t)$ and $i_{cb}(t)$ can be approximated as

$$v_{cb}(t) \approx V_{cb0}\sqrt{1 - \frac{P_o \sin 2\omega t}{{V_{cb0}}^2 C_b \omega}} \tag{9}$$

and

$$i_{cb}(t) \approx \frac{-P_o \cos 2\omega t}{V_{cb0}\sqrt{1 - \frac{P_o \sin 2\omega t}{{V_{cb0}}^2 C_b \omega}}}. \tag{10}$$

B. Flyback Converter With the Additional Rectifier

According to the description in [23], and assuming no power loss in a flyback LED driver operating at DCM, the duty ratio of the magnetizing period is determined by

$$D_y = \frac{2}{V_m}\sqrt{P_o L_p / T_{sw\_m}} \tag{11}$$

where L_p is the magnetizing inductance of the transformer at the primary side and V_m is the magnitude of the input sinusoidal voltage. As shown in Fig. 10(a), the two duty ratios of each

demagnetizing period can be expressed as

$$d_{ro}(t) = \frac{L_p}{{n_t}^2 V_o T_{sw\_m}}[i_{so\_pk}(t) - i_{sb\_pk}(t)],$$
$$d_{rb}(t) = \frac{L_p i_{sb\_pk}(t)}{{n_t}^2 v_{cb}(t) T_{sw\_m}} \tag{12}$$

where $i_{so\_pk}(t)$ and $i_{sb\_pk}(t)$ represent the peak values in one switching period of current $i_{so}(t)$ and $i_{sb}(t)$, respectively. Since the average value of $i_{so}(t)$ for $t \in [T/8, 3T/8]$ can be approximated as the load current, we have

$$d_{ro}(t) i_{so\_pk}(t) - \frac{d_{ro}(t)^2 V_o {n_t}^2 T_{sw\_m}}{2L_p} = I_o. \tag{13}$$

According to [23], we obtain

$$i_{so\_pk}(t) = 2n_t \sqrt{\frac{P_o T_{sw\_m}}{L_p}} |\sin \omega t|. \tag{14}$$

For $t \in [T/8, 3T/8]$, substitution of (14) into (13) yields

$$d_{ro}(t) = \frac{1}{V_o n_t} \sqrt{\frac{P_o L_p}{T_{sw\_m}}} \left(2|\sin \omega t| - \sqrt{-2\cos 2\omega t}\right). \tag{15}$$

Rearranging (12) and substituting (14) and (15) in it for $t \in [T/8, 3T/8]$, we can get

$$d_{rb}(t) = \frac{1}{v_{cb}(t) n_t} \sqrt{\frac{P_o L_p}{T_{sw\_m}}} \sqrt{-2\cos 2\omega t}. \tag{16}$$

To make the flyback converter operate in DCM, (17) should be satisfied for $t \in [T/8, 3T/8]$.

$$D_y + d_{ro}(t) + d_{rb}(t) = \sqrt{\frac{P_o L_p}{T_{sw\_m}}} \left\{ \frac{2}{V_m} + \frac{2}{n_t V_o} |\sin \omega t| + \frac{1}{n_t} \left[\frac{1}{v_{cb}(t)} - \frac{1}{V_o} \right] \sqrt{-2\cos 2\omega t} \right\} \le 1 \tag{17}$$

C. Voltage and Volume of the Storage Capacitor

Instead of (17), a conservative inequality

$$\sqrt{\frac{P_o L_p}{T_{sw\_m}}} \left(\frac{2}{V_m} + \frac{2-\sqrt{2}}{n_t V_o} + \frac{\sqrt{2}}{n_t V_{cb\min}} \right) \le 1 \tag{18}$$

can be used, where $V_{cb\min}$ represents the minimum value of $v_{cb}(t)$. Rearranging (18) yields

$$V_{cb\min} \ge \frac{1}{\frac{n_t}{\sqrt{2}} \sqrt{\frac{T_{sw\_m}}{P_o L_p}} - \frac{n_t \sqrt{2}}{V_m} - \frac{\sqrt{2}-1}{V_o}}. \tag{19}$$

In order to ensure that the LED driver can operate with the entire range of the input voltage, V_m in (19) should be the minimal amplitude of the input ac voltage. The maximum value of $v_{cb}(t)$, namely $V_{cb\max}$, must be lower than V_o. According to (9), the required capacitance C_b and its initial voltage can be obtained as

$$C_b = \frac{2P_o}{\omega({V_{cb\max}}^2 - {V_{cb\min}}^2)}$$
$$V_{cb0} = \sqrt{({V_{cb\max}}^2 + {V_{cb\min}}^2)/2}. \tag{20}$$

In the actual circuit, the voltage and energy flow on capacitor C_b are also related to the size of capacitor C_a. This is because C_a is charged with the energy from C_b through the auxiliary circuit to compensate the voltage ripple on C_b in discharging cycles. This implies that the auxiliary circuit with a smaller C_a is processing lower power. However, C_a also functions as a high-frequency filter for suppressing switching ripple on the output current, and cannot be too small. Considering these two factors, a 20-μF capacitor is used in this paper.

D. Inductance Value of the Auxiliary Circuit

The auxiliary circuit is assumed to be operating in DCM in discharging cycles. As shown in Fig. 12(a), the average input current of the auxiliary circuit over a switching period for $t \in [3T/8, 5T/8]$ can be expressed as

$$i_{ai}(t) = v_{cb}(t) d_a(t)^2 T_{sw\_a}/(2L_a), d_a(t) < [V_o - v_{cb}(t)]/V_o \tag{21}$$

which yields

$$L_a < \frac{v_{cb}(t) T_{sw\_a}}{2 i_{ai}(t)} \left[\frac{V_o - v_{cb}(t)}{V_o} \right]^2. \tag{22}$$

In this equation, $v_{cb}(t)$ can be substituted by (7), and $i_{ai}(t)$ (see Fig. 8) can be expressed as

$$i_{ai}(t) = -i_{cb}(t) - i_b(t) \tag{23}$$

where $i_{cb}(t)$ can be substituted by (8), and $i_b(t)$ is

$$i_b(t) = -p_r(t)/V_o = I_o \cos 2\omega t \tag{24}$$

for $t \in [3T/8, 5T/8]$. The upper bound of inductance L_a defined by (22) is a function of t, and can be plotted with $T_{sw\_a} = 5$ μs, $C_a = 20$ μF, $C_b = 150$ μF, $V_{cb0} = 40$ V, $V_o = 46$ V, $I_o = 0.5$ A, and $\omega = 2\pi \times 60$ rad/s. The plotted curve is shown in Fig. 13. It is observed that the maximum inductance requirement is 20 μH. To enhance the dynamic performance and ease the control design, a 10-μH inductor is used in the experiment.

IV. Efficiency Comparison

The power processed by the auxiliary circuit can be expressed as

$$p_a(t) = v_{cb}(t) i_{ai}(t) \tag{25}$$

where $v_{cb}(t)$ and $i_{ai}(t)$ are explained in (7) and (23), respectively. The curves that represent the power processed by the proposed and other auxiliary circuits are plotted in Fig. 14, using (25) or according to [23] and [32]. The buck–boost circuit in [23], the full-bridge circuit in [32], and the proposed unidirectional auxiliary circuit are denoted as circuits I, II, and III, respectively. In this case, the power processed by circuits II and III are comparable and much lower (about 8% of that processed

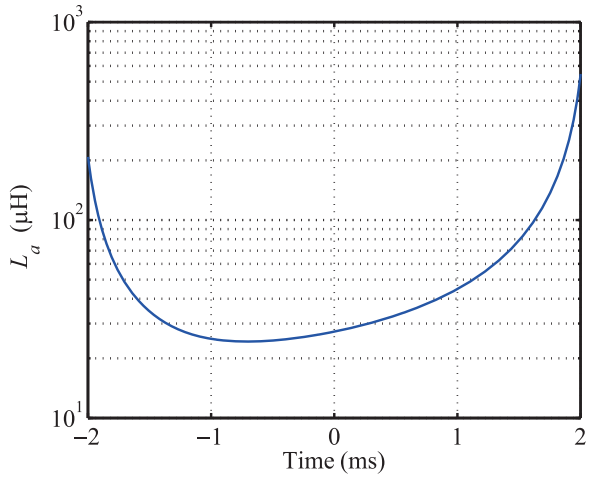

Fig. 13. Required maximum inductance value of L_a in one discharging cycle.

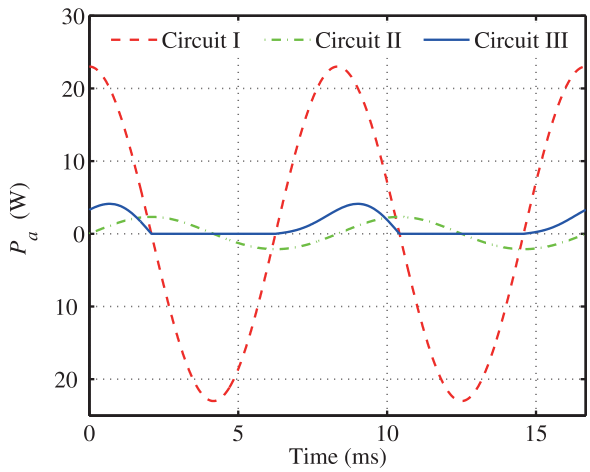

Fig. 14. Instantaneous power processed by the three circuits for power ripple isolation in one period of the input ac voltage. Circuit I represents a bidirectional buck–boost circuit presented in [23] and shown in Fig. 2. Circuit II represents a bidirectional full-bridge circuit presented in [32] and shown in Fig. 4. Circuit III represents the proposed unidirectional auxiliary circuit.

by circuit I). The explanations for this are as follows. The output power of the auxiliary circuit is $v_{ca}(t)i_{ao}(t)$. Since voltage $v_{ca}(t)$ is much lower than V_o and current $i_{ao}(t)$ is slightly higher than $i_b(t)$, the operating power of the auxiliary circuit is only a small fraction of the ripple power $V_o i_b(t)$. Furthermore, the mean value of power loss from circuit III can be derived as

$$P_{a\_loss} = W_a\omega/\pi \cdot (1/\eta_a - 1), W_a = \int_{3T/8}^{5T/8} p_a(t)dt \quad (26)$$

for a given efficiency η_a. A comparison of P_{a_loss} from the three circuits is shown in Fig. 15, which implies that circuits II and III will not significantly lower the efficiency of the LED driver even if they are not very efficient.

Note that the additional power loss from the additional rectifier is not considered. Because switch Q_b has much lower turn-on resistance than that of rectifier diode D_{sb}, the added conduction loss by Q_b is negligible. In addition, the voltage on

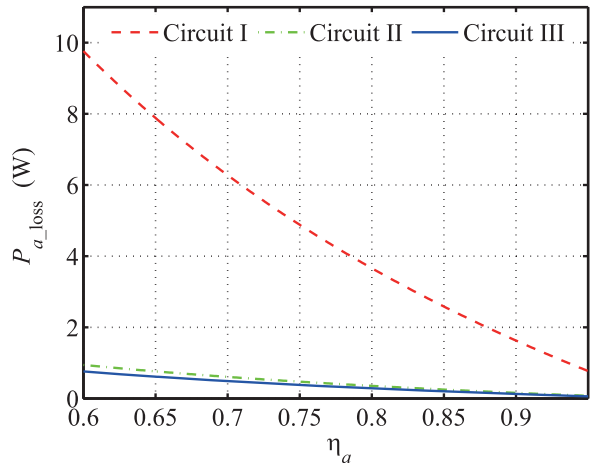

Fig. 15. Power loss from the auxiliary circuits vary with their efficiencies.

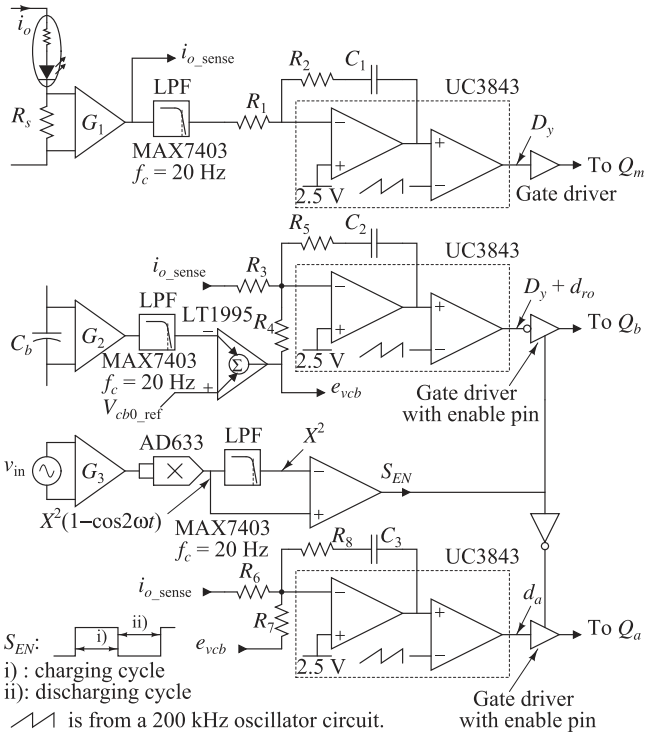

Fig. 16. Schematic diagram of the controller for the proposed LED driver.

Q_b is close to the level of v_{ca}, which is very low. Therefore, the switching loss is neglected in this paper.

V. Controller Design

A simplified diagram depicting an analog implementation of the controller for the proposed LED driver is shown in Fig. 16. The controller senses the load current, the voltage of the capacitor C_b, and the input voltage to control three switches, Q_m, Q_b, and Q_a in the power stage. A general proportional-integral (PI) control scheme is used to regulate the output power of the flyback converter and manage the additional rectifier and the unidirectional auxiliary circuit.

A. Control Design of the Flyback Converter

A PI unit is used to control the turn-on duty ratio of the main switch in the flyback converter to regulate the load current that is sensed by a current shunt resistor R_s and a differential amplifier circuit G_1. The output signal of G_1 denoted by i_{o_sense} is fed into a low-pass filter (LPF) implemented by the LPF IC MAX7403. The filtered signal is subtracted from the reference, and the difference is processed by a PI unit. Next, the duty-ratio signal D_y is generated according to the following traditional PI control expression:

$$D_y = K_{p1}(I_{o\_\mathrm{ref}} - i_{o\_\mathrm{LPF}}) + K_{i1}\int (I_{o\_\mathrm{ref}} - i_{o\_\mathrm{LPF}})dt \tag{27}$$

where I_{o_ref} and i_{o_LPF} represent the reference and the mean value of the load current, respectively. In the experiment, $K_{p1} = 1.5 \times 10^{-3}$ and $K_{i1} = 1.1$. The pulsewidth-modulation (PWM) signal that is generated by a modulator with a sawtooth-wave clock drives the switch Q_m through a gate-driver circuit. The PI control unit with the PWM signal generator is realized by the PWM controller UC3843.

B. Control Design of the Additional Rectifier

In the charging cycles, the turn-on time of the additional rectifier is controlled to regulate the load current and the mean value of the capacitor voltage v_{cb} that is sensed and scaled down by a differential amplifier circuit G_2. Then, the sampled v_{cb} is processed by a LPF and then subtracted from its reference through the subtractor implemented by the amplifier IC LT1995. Then, the voltage-error signal $e_{vcb} = A_{vcb}(V_{cb0\_\mathrm{ref}} - v_{cb\_\mathrm{LPF}})$ is generated (A_{vcb} is the attenuation factor of sensing circuits, V_{cb0_ref} is the reference for V_{cb0} value, and v_{cb_LPF} is the mean value of v_{cb}). The voltage-error signal e_{vcb} and the current signal i_{o_sense} are separately fed into the PI unit through resistors R_4 and R_3. The duty-ratio signal of the additional rectifier is generated according to

$$\begin{aligned} D_y + d_{ro} = {} & K_{p2}(I_{o\_\mathrm{ref}} - i_o) + K_{i2}\int (I_{o\_\mathrm{ref}} - i_o)dt \\ & + K_{vcb1}K_{p2}(v_{cb\_\mathrm{LPF}} - V_{cb0\_\mathrm{ref}}) \\ & + K_{vcb1}K_{i2}\int (v_{cb\_\mathrm{LPF}} - V_{cb0\_\mathrm{ref}})dt \end{aligned} \tag{28}$$

where $K_{p2} = 3.15$, $K_{i2} = 23.3 \times 10^3$, and $K_{vcb1} = 0.029$. Since perturbations on v_{cb} are slow, a very small factor K_{vcb1} is used. The PWM signal generated by the controller drives switch Q_b through an inverting gate driver, and its turn-on duration is $[1 - (D_y + d_{ro})]T_{sw\_m}$. Note that the clock used to generate this PWM signal must also be the same as that used in the flyback converter control.

C. Control Design of the Auxiliary Circuit

In the discharging cycles, the auxiliary circuit operates to manage the load current and the capacitor voltage v_{cb}. Its control design includes one PI unit with a modulator, similar to the one used for the additional rectifier, as shown in Fig. 16. The inputs are signals i_{o_sense} and e_{vcb}. The duty-ratio signal d_a is generated according to the formula

$$\begin{aligned} d_a = {} & K_{p3}(I_{o\_\mathrm{ref}} - i_o) + K_{i3}\int (I_{o\_\mathrm{ref}} - i_o)dt \\ & + K_{vcb2}K_{p3}(v_{cb\_\mathrm{LPF}} - V_{cb0\_\mathrm{ref}}) \\ & + K_{vcb2}K_{i3}\int (v_{cb\_\mathrm{LPF}} - V_{cb0\_\mathrm{ref}})dt \end{aligned} \tag{29}$$

where $K_{p3} = 1.07$, $K_{i3} = 15.0 \times 10^3$, and $K_{vcb2} = 0.026$. The PWM signal with the duty ratio d_a is fed into a noninverting gate driver that is driving Q_m.

TABLE II
PARAMETERS VALUES AND COMPONENT PART NUMBERS OF THE PROTOTYPE

Parameter/component		Value/part number
Input voltage		90–240 V/60 Hz
Output voltage/current (full load)		46 V/0.5 A
Loads		High-flux LED CXA1304 × 5
Diode bridge		DF04S
Transformer	Magnetic core	RM10
	Turns ratio (n_t)	2
	Magnetizing inductance (L_p)	80 μH
MOSFET	Q_m	C2M0080120D
	Q_a, Q_b	TK7S10N1Z
Diodes	D_{so}, D_{sb}, D_a	C3D02060E
Inductor	L_a	10 μH
	L_o	33 μH
Capacitor	C_a	20 μF
	C_b	100–300 μF
Switching frequency	f_{sw_m}, f_{sw_a}	200 kHz

D. Switch Enable Signal

Since the additional rectifier and the auxiliary circuit alternately operate in different periods of time, a signal S_{EN} is used to enable the switch that is to operate. The input ac voltage is sensed and scaled down by differential amplifier G_3. Then, the input-voltage signal is squared and fed into the LPF, yielding a pulsating signal $X^2(1 - \cos 2\omega t)$ having a mean value X^2. Subsequently, the S_{EN} signal is generated by comparing the signals mentioned above, and will be logic high during charging cycles or low during discharging cycles. The gate-driver circuits for switches Q_b and Q_a are, respectively, enabled by S_{EN} and its inverted signal.

VI. EXPERIMENTAL VERIFICATION

A prototype with high-flux LED loads has been built to verify the proposed LED driver, as shown in Fig. 8. The parameter values and part numbers of the components in the prototype are shown in Table II. The required minimum storage capacitance (C_b) is 83 μF, and the associated operating voltage of the capacitor is 23.5–45 V, which is determined by the parameters of the flyback converter, and (19) and (20). Note that the switching frequency of the flyback converter with the additional active rectifier should be set as low as possible to reduce the switching loss. However, the auxiliary circuit may operate at a higher frequency to obtain faster response to the ripple power.

TABLE III
FOUR CONFIGURATIONS OF THE PROTOTYPE IN EXPERIMENTS

Configuration	Topology and storage capacitors	Voltage of the storage capacitor	
		v_{cb} (for full load)	V_{cb0}
Config. I	Conventional flyback converter (see Fig. 1), 3300-μF aluminum E-cap		
Config. II	Proposed topology with additional 300-μF polymer-hybrid capacitors	37 V–43 V	$V_{cb0} = 40$ V
		32.5 V–39 V	$V_{cb0} = 36$ V
Config. III	circuits 156-μF polymer-hybrid capacitors	33 V–45 V	$V_{cb0} = 39$ V
Config. IV	(see Fig. 8) approximately 100-μF ceramic capacitors	26 V–46 V	$V_{cb0} = 36$ V

In the prototype, one 200-kHz clock signal is used to simplify the control circuit. This frequency is determined by considering the capability of the MOSFETS and their gate-driver circuits.

To comprehensively evaluate the performance of the proposed LED driver, four configurations of the prototype are tested with different storage capacitance. In Config. I, the prototype is operating as a conventional flyback ac–dc LED driver shown in Fig. 1, with a 3300-μF aluminum E-cap connected to the output port. In Config. II, the proposed additional circuits and two small capacitors are connected (see Fig. 8), and the capacitance C_b is 300 μF, which is realized by three 100-μF polymer-hybrid capacitors with long lifespan and compact size. In Config. III, the storage capacitance is reduced to 156 μF. In Config. IV, a 100-μF ceramic capacitor bank is used for energy storage. Because the capacitance drift is significant when the voltage of ceramic capacitors is close to their rating level [37], 90 ceramic capacitors are connected in parallel to achieve the required equivalent capacitance. With Config. IV, a long-life and compact E-cap-less LED driver can be realized. The description of the configurations are summarized in Table III. The photos of the prototype with different storage capacitors are shown in Fig. 17. Note that the prototype occupies much larger space than commercialized LED drivers with the same power level. This is because many analog components are used in the controller. However, these circuits may be integrated as a single IC, or the controller can be implemented by a digital signal processor circuit. In that case, the size will be significantly reduced. In addition, the transformer is over designed, and its size can be further reduced for commercialization.

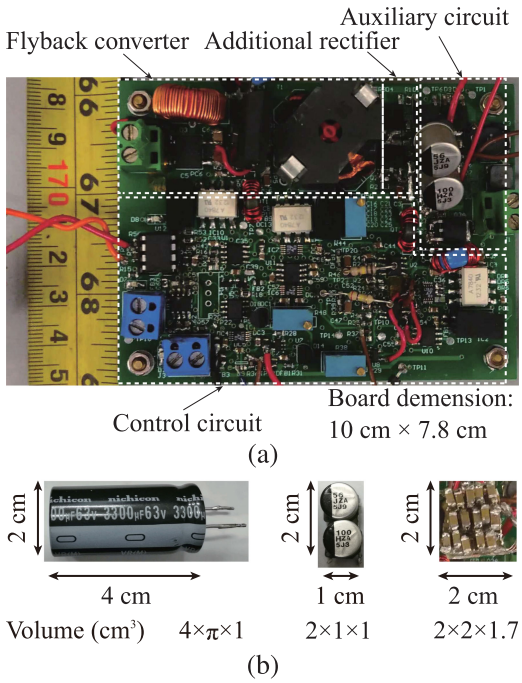

Fig. 17. Prototype photograph with dimension indicators for the board and the capacitors for different configurations. (a) Proposed LED driver with Config. III. (b) Aluminum E-cap for Config. I, the polymer-hybrid capacitors for Config. III, and the ceramic capacitors with 10-μF capacitance, 50-V voltage rating, and 1206 package for Config. IV.

A. Experimental Waveforms

The experimental waveforms of the LED driver with Configs. I and II at the full-load condition are shown in Fig. 18. The load current i_o of the LED driver with Config. I contains a peak-to-peak 50-mA 120-Hz ripple, as shown in Fig. 18(a). However, in the proposed LED driver with Config. II, the output current contains very low ripple although the voltage ripple on the storage capacitor C_b is substantial, as shown in Fig. 18(b) and (c). The input current and voltage are in phase, because the additional circuit installed at the load side does not affect the flyback converter operating. The waveforms for the LED driver operating at the half-load condition are given in Fig. 19.

The key waveforms of the proposed LED driver with Config. II are shown in Figs. 20 and 21. It is observed from these figures that the auxiliary circuit operates (the current i_{La} is nonzero) only in discharging cycles, with energy flowing from C_b to C_a. The operating voltage of the capacitors are set at different levels. At the full-load condition, the voltage v_{cb} is varying from 37 to 43 V when $V_{cb0} = 40$ V, and the voltage v_{ca} is correspondingly varying from 9 to 3 V, as shown in Fig. 20(a). When $V_{cb0} = 36$ V, v_{cb} is varying from 32.5 to 39 V. Correspondingly, v_{ca} varies from 13 to 6.5 V, as shown in Fig. 20(b). Thereby, the voltage of $v_{cb} + v_{ca}$ is kept as 46 V, and the load current regulation is achieved. Similarly, the load voltage is kept at 44 V with the load regulated at its half level, as shown in Fig. 21. The key waveforms of the proposed LED driver in a short-time scale are shown in Fig. 22. The waveforms of the LED driver with Config. III are shown in Fig. 23, where larger voltage variations are observed due to a smaller storage capacitor.

The waveforms of the LED driver with Config. IV are shown in Fig. 24. As compared with the waveforms in Figs. 20, 21, and 23, voltage v_{cb} contains the largest ripple (26-to-46 V), because of the low equivalent storage capacitance (about 100 μF) in

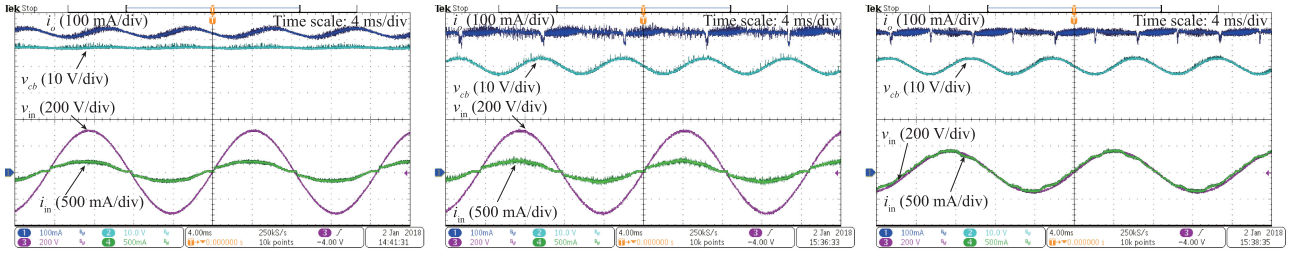

Fig. 18. Input voltage $v_{\rm in}$ and current $i_{\rm in}$, output current i_o, and the voltage of storage capacitor v_{cb} in the LED driver with (a) Config. I ($v_{\rm in\_rms} = 220$ V), (b) Config. II ($v_{\rm in\_rms} = 220$ V), and (c) Config. II ($v_{\rm in\_rms} = 110$ V) at the full-load condition ($i_o = 0.5$ A).

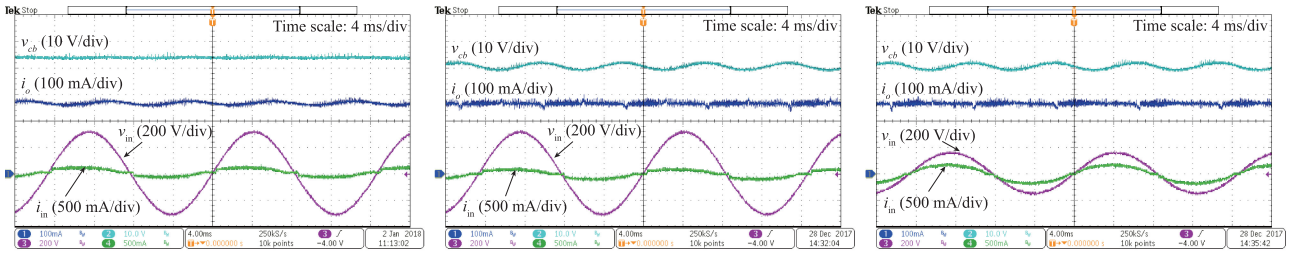

Fig. 19. Input voltage $v_{\rm in}$ and current $i_{\rm in}$, output current i_o, and the voltage of storage capacitor v_{cb} in the LED driver with (a) Config. I ($v_{\rm in\_rms} = 220$ V), (b) Config. II ($v_{\rm in\_rms} = 220$ V), and (c) Config. II ($v_{\rm in\_rms} = 110$ V) at the half-load condition ($i_o = 0.25$ A).

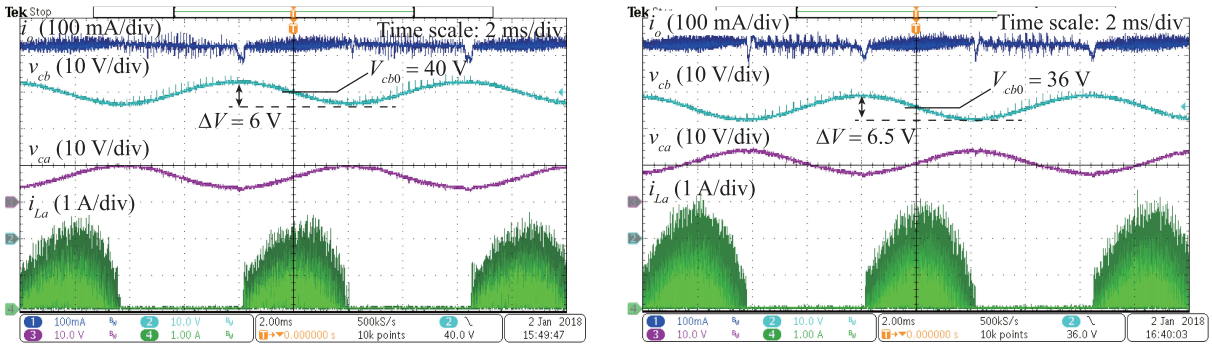

Fig. 20. Capacitor voltages v_{cb} and v_{ca}, inductor current i_{La}, and output current i_o of the proposed LED driver with Config. II. (a) $V_{cb0} = 40$ V. (b) $V_{cb0} = 36$ V at the full-load condition.

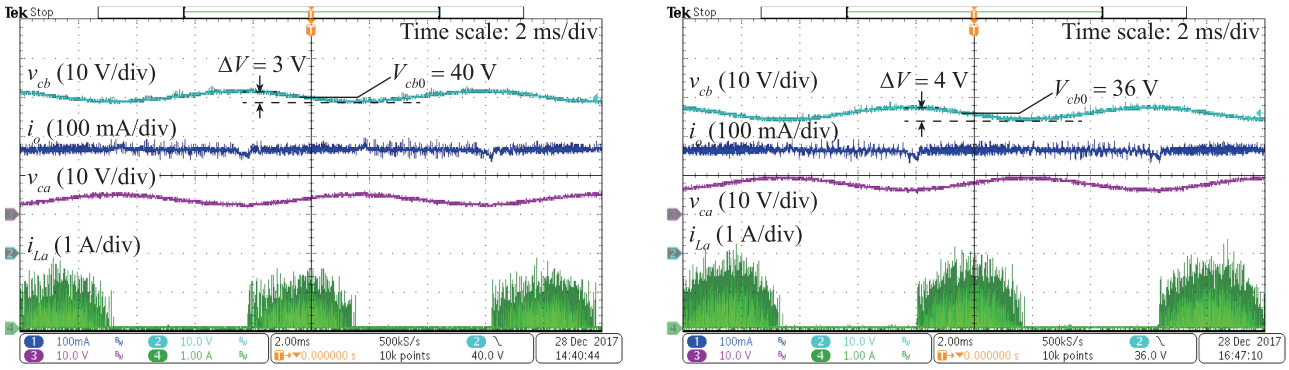

Fig. 21. Capacitor voltages v_{cb} and v_{ca}, inductor current i_{La}, and output current i_o of the proposed LED driver with Config. II. (a) $V_{cb0} = 40$ V. (b) $V_{cb0} = 36$ V at the half-load condition.

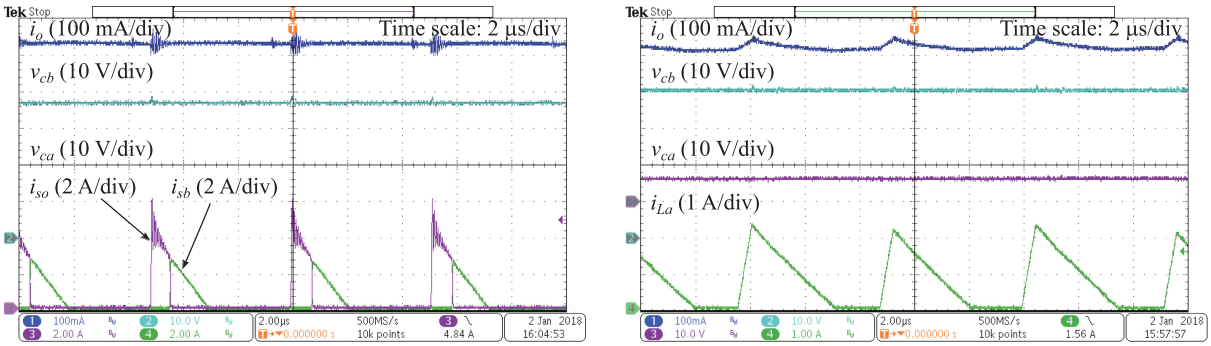

Fig. 22. Waveforms in a short time scale in the proposed LED driver with Config. II. (a) Transformer secondary current (i_{so}, i_{sb}). (b) Inductor current (i_{La}) in auxiliary circuit.

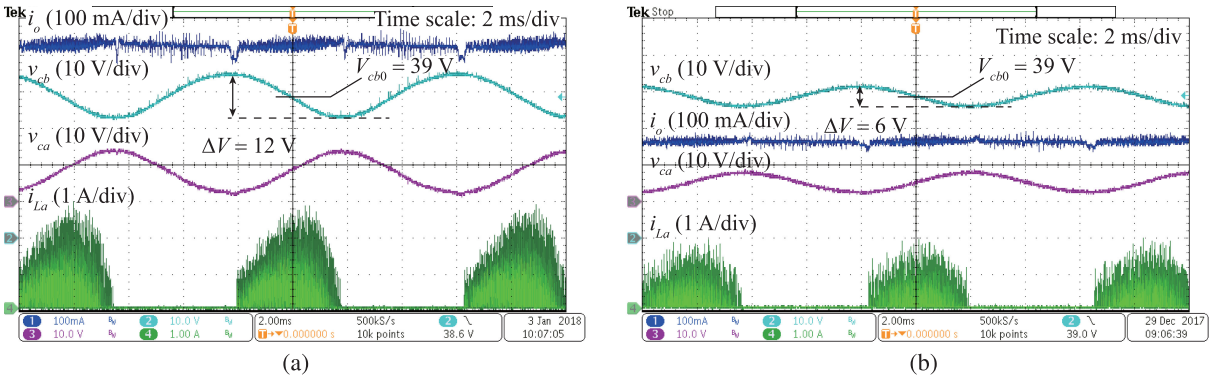

Fig. 23. Capacitor voltages v_{cb} and v_{ca}, inductor current i_{La}, and output current i_o of the proposed LED driver with Config. III. (a) Full-load condition. (b) Half-load condition.

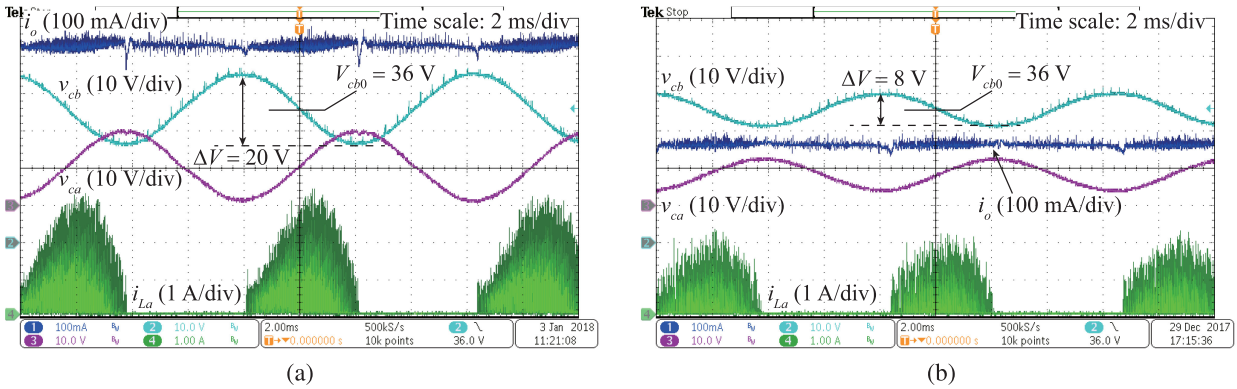

Fig. 24. Capacitor voltages v_{cb} and v_{ca}, inductor current i_{La}, and output current i_o of the proposed LED driver with Config. IV. (a) Full-load condition. (b) Half-load condition.

this configuration. In addition, spikes periodically appear on current i_o as the auxiliary circuit stops operating, which can be improved with control optimization. Specifically, the duty ratio of the auxiliary circuit needs to swiftly change to follow the large variation of the input power and the capacitor voltages. However, the duty-ratio signal is directly generated by a PI controller, which cannot offer such fast dynamic response. For this reason, the output current i_o is not ideally regulated, and apparent deviations occur at the end and beginning of each discharging cycle. This can be solved by using a feedforward-based control scheme shown in Fig. 25. In that

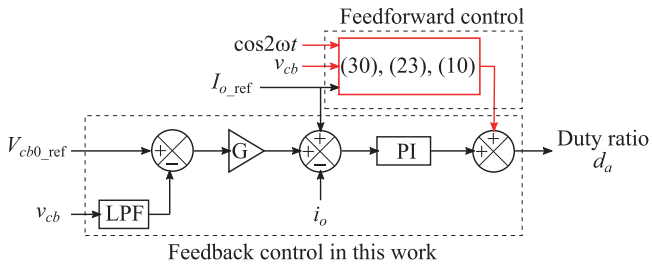

Fig. 25. Feedforward control scheme for improving the dynamic response of the auxiliary circuit in the proposed LED driver.

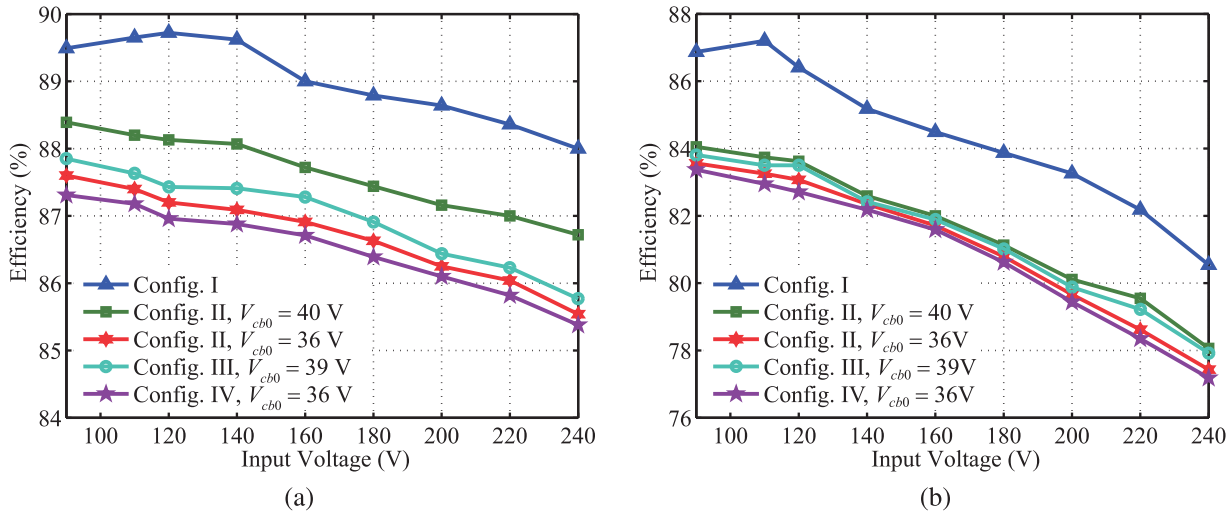

Fig. 26. Efficiency comparison of the LED driver with different configurations and parameters. (a) Full-load condition. (b) Half-load condition.

TABLE IV
EFFICIENCY COMPARISON AMONG THE PROPOSED LED DRIVER AND OTHER SIMILAR DESIGNS

LED driver	Ref.	Operating voltage (V)	Efficiency	Efficiency reduction from the auxiliary circuit
Fig. 2	[23]	90–264	Full load: 87.8%–86.8%	3.2%–2.5%
	[24]	90–264	Full load: 87%–86.5%	4%–3.7%
	[26]	90–264	Full load: 81%–77%	Not reported
Fig. 3	[27]	100–220	Full load: 66%–60%	Not reported
	[28]	110–220	Full load: 80%–76%	Not reported
	[29]	100–260	Full load: 89.5%–85.2%	Not reported
	[30]	90–265	Full load: 87.5%–80%	Not reported
	[31]	85–130	Full load: 90%–89.9% 1/3 load: 82%–80%	1.34% @ $V_{\rm in}$ = 110 V
Fig. 4	[32]	90–264	Full load: 92.2%–89.9%	1.1%–0.59%
	[33]	90–264	Full load: 92.4%–89.8%	1.23%–0.54%
Fig. 5	[34]	110–230	Full load: 85.6%–85.5%	1%–0.9%
Fig. 6	[35]	110–220	Full load: 86%–83%	Not reported
Proposed LED driver (Config. I and V_{cb0} = 40 V)		90–240	Full load: 88.4%–86.7% Half load: 84%–78%	Full load: 1.6%–1% Half load: 3.4%–2.4%

case, the duty-ratio signal will be dominated by the feedforward signal that is generated with

$$d_a(t) = \sqrt{\frac{2i_{ai}(t)L_a}{v_{cb}(t)T_{sw\_a}}} \text{ for } t \in [3T/8, 5T/8] \qquad (30)$$

and other associated equations, and the calculation error can be compensated by a PI controller.

B. Experimental Efficiency Analysis

The efficiency of the prototype with different configurations, line voltages, and load conditions are shown in Fig. 26. The traditional flyback LED driver achieves a much lower efficiency (89.7%–88% for the full load and 87.2%–80.5% for the half load) than most commercially available LED drivers. However, the prototype can be further improved, e.g., by optimizing the magnetic design to reduce the transformer leakage inductance. Since this paper focuses on the ripple power decoupling, the prototype with such efficiency can be used to verify the proposed design.

A comparison among the proposed LED driver and other alternates in the literature in terms of efficiency is shown in Table IV. For the full-load efficiency, the proposed LED driver is better than most designs in the table. In addition, the efficiency reduction from the auxiliary circuit with Config. II and V_{cb0} = 40 V is comparable to the value achieved in [32]–[34] at the full-load condition, which verifies the low power processing on it. Note that, in the worst case, the efficiency reduction is up to 2.8% at the full-load condition, or 4.1% at the half-load condition (see Fig. 26). Nevertheless, there is still a large room for enhancing the efficiency. For example, the conduction loss and the magnetic loss on the auxiliary circuit can be further reduced by operating it at continuous-conduction mode instead of DCM.

Moreover, it is observed that a lower voltage on C_b leads to a lower efficiency from comparison between the two curves associated with Config. II. It is concluded that V_{cb0} value should be set as high as possible. In addition, a lower capacitance of C_b results in a lower efficiency by comparing the curves associated with Config. II (V_{cb0} = 40 V) and Config. III (V_{cb0} = 39 V). However, higher capacitance means higher cost on capacitors

and larger space occupied by them. There will be a tradeoff between the size or cost and the efficiency of the proposed LED driver.

VII. Conclusion

In traditional ac–dc LED drivers, a large storage capacitor is required to buffer double-line-frequency power ripple from the ac source, which may limit the lifetime of LED lamps or add cost to the lighting systems. Previous works have shown that a dedicated bidirectional auxiliary circuit can be used to isolate the ripple power with a lower capacitance requirement. This paper proposes an LED driver with an additional active rectifier and a unidirectional auxiliary circuit that processes very low power (about 8% of the ripple power). Compared with previous similar designs, the proposed auxiliary circuit operates at a lower voltage and consists of fewer components, which can lower the cost and ease the circuit design. In the experiment, the prototype with various low-volume and long-lifespan capacitors is tested. An efficiency comparison of the LED driver with various configurations is given.

References

[1] S. Li, S. C. Tan, C. K. Lee, E. Waffenschmidt, S. Y. R. Hui, and C. K. Tse, "A survey, classification, and critical review of light-emitting diode drivers," *IEEE Trans. Power Electron.*, vol. 31, no. 2, pp. 1503–1516, Feb. 2016.

[2] A. Shagerdmootaab and M. Moallem, "Filter capacitor minimization in a flyback LED driver considering input current harmonics and light flicker characteristics," *IEEE Trans. Power Electron.*, vol. 30, no. 8, pp. 4467–4476, Aug. 2015.

[3] 2012. [Online]. Available: https://www.usa.philips.com/

[4] N. Narendran and Y. Gu, "Life of LED-based white light sources," *J. Display Technol.*, vol. 1, no. 1, pp. 167–171, Sep. 2005.

[5] M. Arias, A. Vazquez, and J. Sebastián, "An overview of the AC-DC and DC-DC converters for LED lighting applications," *Autom. J. Control Meas. Electron. Comput. Commun.*, vol. 53, no. 2, pp. 156–172, May 2012.

[6] P. T. Krein, R. S. Balog, and M. Mirjafari, "Minimum energy and capacitance requirements for single-phase inverters and rectifiers using a ripple port," *IEEE Trans. Power Electron.*, vol. 27, no. 11, pp. 4690–4698, Nov. 2012.

[7] A. Wilkins, J. Veitch, and B. Lehman, "LED lighting flicker and potential health concerns: IEEE standard PAR1789 update," in *Proc. IEEE Energy Convers. Congr. Expo.*, 2010, pp. 171–178.

[8] B. Lehman, A. Wilkins, S. Berman, M. Poplawski, and N. J. Miller, "Proposing measures of flicker in the low frequencies for lighting applications," in *Proc. IEEE Energy Convers. Congr. Expo.*, 2011, pp. 2865–2872.

[9] B. Lehman and A. J. Wilkins, "Designing to mitigate effects of flicker in LED lighting: Reducing risks to health and safety," *IEEE Power Electron. Mag.*, vol. 1, no. 3, pp. 18–26, Sep. 2014.

[10] Useful Life: Understanding LM-80, Lumen maintenance, and LED fixture lifetime. (2010). [Online]. Available: http://www.colorkinetics.com/support/whitepapers/LEDLifetime.pdf

[11] Axial and radial aluminum electrolytic capacitors: Up to 150 °C for demanding vehicular, lighting and other long-life applications, KEMET, Simpsonville, SC, USA, 2014. [Online]. Available: http://www.kemet.com/Lists/ProductCatalog/Attachments/424/KEM_AC102.pdf

[12] Capacitor selection guide, KEMET, Simpsonville, SC, USA, 2015. [Online]. Available: http://www.kemet.com/Lists/FileStore/Capacitor%20Selection%20Guide.pdf

[13] S. Zhao, X. Ge, X. Wu, J. Zhang, and H. Zhang, "Analysis and design considerations of two-stage AC-DC LED driver without electrolytic capacitor," in *Proc. IEEE Energy Convers. Cong. Expo.*, 2014, pp. 2606–2610.

[14] C. K. Tse, M. H. L. Chow, and M. K. H. Cheung, "A family of PFC voltage regulator configurations with reduced redundant power processing," *IEEE Trans. Power Electron.*, vol. 16, no. 6, pp. 794–802, Nov. 2001.

[15] L. Gu, X. Ruan, M. Xu, and K. Yao, "Means of eliminating electrolytic capacitor in AC/DC power supplies for LED lightings," *IEEE Trans. Power Electron.*, vol. 24, no. 5, pp. 1399–1408, May 2009.

[16] B. Wang, X. Ruan, K. Yao, and M. Xu, "A method of reducing the peak-to-average ratio of LED current for electrolytic capacitor-less AC-DC drivers," *IEEE Trans. Power Electron.*, vol. 25, no. 3, pp. 592–601, Mar. 2010.

[17] X. Ruan, B. Wang, K. Yao, and S. Wang, "Optimum injected current harmonics to minimize peak-to-average ratio of LED current for electrolytic capacitor-less AC-DC drivers," *IEEE Trans. Power Electron.*, vol. 26, no. 7, pp. 1820–1825, Jul. 2011.

[18] C. S. Wong, Y. M. Lai, K. H. Loo, and C. K. Tse, "Low-current ripple LED driver by two-phase driving approach," *IET Electron. Lett.*, vol. 51, no. 22, pp. 1804–1806, Oct. 2015.

[19] J. C. W. Lam and P. K. Jain, "A high power factor, electrolytic capacitor-less AC-input LED driver topology with high frequency pulsating output current," *IEEE Trans. Power Electron.*, vol. 30, no. 2, pp. 943–955, Feb. 2015.

[20] J. C. W. Lam and P. K. Jain, "Isolated AC/DC offline high power factor single-switch LED drivers without electrolytic capacitors," *IEEE J. Emerg. Sel. Topics Power Electron.*, vol. 3, no. 3, pp. 679–690, Sep. 2015.

[21] B. White, H. Wang, Y.-F. Liu, and X. Liu, "An average current modulation method for single-stage LED drivers with high power factor and zero low-frequency current ripple," *IEEE J. Emerg. Sel. Topics Power Electron.*, vol. 3, no. 3, pp. 714–731, Sep. 2015.

[22] W.-K. Lun, K. H. Loo, S. C. Tan, Y. M. Lai, and C. K. Tse, "Bi-level current driving technique for LEDs," *IEEE Trans. Power Electron.*, vol. 24, no. 12, pp. 2920–2932, Dec. 2009.

[23] S. Wang, X. Ruan, K. Yao, S. C. Tan, Y. Yang, and Z. Ye, "A flicker-free electrolytic capacitor-less AC–DC LED driver," *IEEE Trans. Power Electron.*, vol. 27, no. 11, pp. 4540–4548, Nov. 2012.

[24] Y. Yang, X. Ruan, L. Zhang, J. He, and Z. Ye, "A feed-forward scheme for an electrolytic capacitor-less AC/DC LED driver to reduce output current ripple," *IEEE Trans. Power Electron.*, vol. 29, no. 10, pp. 5508–5517, Oct. 2014.

[25] K.-W. Lee, Y.-H. Hsieh, and T.-J. Liang, "A current ripple cancellation circuit for electrolytic capacitor-less AC-DC LED driver," in *Proc. 28th Annu. IEEE Appl. Power Electron. Conf. Expo.*, 2013, pp. 1058–1061.

[26] Y. Zhang and K. Jin, "A single-stage electrolytic capacitor-less AC/DC LED driver," in *Proc. IEEE Power Electron. Appl. Conf. Expo.*, 2014, pp. 881–886.

[27] F. Wang, L. Li, Y. Zhong, and X. Shu, "Flyback-based three-port topologies for electrolytic capacitor-less LED drivers," *IEEE Trans. Ind. Electron.*, vol. 64, no. 7, pp. 5818–5827, Jul. 2017.

[28] W. Chen and S. Y. R. Hui, "Elimination of an electrolytic capacitor in AC/DC light-emitting diode (LED) driver with high input power factor and constant output current," *IEEE Trans. Power Electron.*, vol. 27, no. 3, pp. 1598–1607, Mar. 2012.

[29] H. Valipour, G. Rezazadeh, and M. R. Zolghadri, "Flicker-free electrolytic capacitor-less universal input offline LED driver with PFC," *IEEE Trans. Power Electron.*, vol. 31, no. 9, pp. 6553–6561, Sep. 2016.

[30] H. Dong, X. Xie, L. Jiang, and Z. Jin, "An electrolytic capacitor-less high power factor LED driver based on a "One-and-a-Half Stage" Forward-flyback topology," *IEEE Trans. Power Electron.*, vol. 33, no. 2, pp. 1572–1584, Feb. 2018.

[31] H. Wu, S.-C. Wong, C. K. Tse, S. Y. R. Hui, and Q. Chen, "Single-phase LED drivers with minimal power processing, constant output current, input power factor correction, and without electrolytic capacitor," *IEEE Trans. Power Electron.*, vol. 33, no. 7, pp. 6159–6170, Jul. 2018.

[32] Y. Qiu, H. Wang, L. Wang, Y.-F. Liu, and P. C. Sen, "Current-ripple-based control strategy to achieve low-frequency ripple cancellation in single-stage high-power LED driver," in *Proc. IEEE Energy Convers. Cong. Expo.*, 2015, pp. 5316–5322.

[33] Y. Qiu, L. Wang, H. Wang, Y.-F. Liu, and P. C. Sen, "Bipolar ripple cancellation method to achieve single-stage electrolytic-capacitor-less high-power LED driver," *IEEE J. Emerg. Sel. Topics Power Electron.*, vol. 3, no. 3, pp. 698–713, Sep. 2015.

[34] P. Fang, Y.-F. Liu, and P. C. Sen, "A flicker-free single-stage offline LED driver with high power factor," *IEEE J. Emerg. Sel. Topics Power Electron.*, vol. 3, no. 3, pp. 654–665, Sep. 2015.

[35] P. Fang and Y.-F. Liu, "Energy channeling LED driver technology to achieve flicker-free operation with true single stage power factor correction," *IEEE Trans. Power Electron.*, vol. 32, no. 5, pp. 3892–3907, May 2017.
[36] G. L. Brainard, "Non-dissipative battery charger equalizer," U.S. Patent 5479083, Dec. 26, 1995.
[37] C. B. Barth, I. Moon, Y. Lei, S. Qin, and R. C. N. Pilawa-Podgurski, "Experimental evaluation of capacitors for power buffering in single-phase power converters," in *Proc. IEEE Energy Convers. Cong. Expo.*, 2015, pp. 6269–6276.

Zhenyu Shan (S'10–M'13) received the B.Eng. and M.Eng. degrees in control engineering from Beijing Jiaotong University, Beijing, China, in 2007 and 2009, respectively, and the Ph.D. degree in power electronics from Hong Kong Polytechnic University, Hong Kong, in 2013.

He was a Visiting Student with the Grainger Center for Electric Machinery and Electromechanics, University of Illinois at Urbana-Champaign, Champaign, IL, USA, from March to June 2013. He joined the North China University of Technology, Beijing, China, in December 2016, as a University High-level Talent and an Assistant Professor with the Department of Electrical Engineering. He was a Postdoctoral Research Fellow with the Department of Electrical and Computer Engineering, University of British Columbia, Vancouver, BC, Canada, from November 2013 to June 2016. His research interests include PFC converters, ac–dc LED drivers, power converter modeling and nonlinear control, and converter-based ac–dc systems.

Dr. Shan serves as a Reviewer for various IEEE transactions and other international journals on electrical and electronic engineering.

Xiaomei Chen received the B.S. degree in electrical engineering and automation from the North China University of Technology, Beijing, China, in 2017, where she is currently working toward the M.S. degree in electrical engineering.

Her current research interests include ac–dc converters and LED drivers.

Juri Jatskevich (M'99–SM'07–F'17) received the M.S.E.E. and the Ph.D. degrees in electrical engineering from Purdue University, West Lafayette IN, USA, in 1997 and 1999, respectively.

Since 2002, he has been a Faculty Member with the University of British Columbia, Vancouver, BC, Canada, where he is currently a Professor of electrical and computer engineering. His research interests include power electronic systems, electrical machines and drives, and modeling and simulation of electromagnetic transients.

Dr. Jatskevich has served as an Associate Editor for the IEEE TRANSACTIONS ON POWER ELECTRONICS for the period 2008–2013, and is currently the Editor-in-Chief of the IEEE TRANSACTIONS ON ENERGY CONVERSION, and Editor of the IEEE POWER ENGINEERING LETTERS. He Chaired the IEEE CAS Power Systems & Power Electronic Circuits Technical Committee in 2009–2010. He is also chairing the IEEE Task Force on Dynamic Average Modeling, under Working Group on Modeling and Analysis of System Transients Using Digital Programs.

Chi K. Tse (M'90–SM'97–F'06) received the B.Eng. (Hons.) degree (first class Hons.) in electrical engineering and the Ph.D. degree from the University of Melbourne, Melbourne, VIC, Australia, in 1987 and 1991, respectively.

He is currently a Chair Professor with Hong Kong Polytechnic University, Hong Kong, with which he served as the Head of the Department of Electronic and Information Engineering from 2005 to 2012. His research interests include power electronics, nonlinear systems, and complex network applications.

Dr. Tse was the recipient of a number of research and industry awards, including the Prize Paper Awards by the IEEE TRANSACTIONS ON POWER ELECTRONICS in 2001 and 2015, the RISP Journal of Signal Processing Best Paper Award in 2014, the Best Paper Award by the *International Journal of Circuit Theory and Applications* in 2003, two Gold Medals at the International Inventions Exhibition in Geneva in 2009 and 2013, a Silver Medal at the International Invention Innovation Competition in Canada in 2016, and a number of recognitions by the academic and research communities, including honorary professorship by several Chinese and Australian universities, Chang Jiang Scholar Chair Professorship, IEEE Distinguished Lectureship, Distinguished Research Fellowship by the University of Calgary, Gledden Fellowship, and International Distinguished Professorship-at-Large by the University of Western Australia. While with the Hong Kong Polytechnic University, he received the President's Award for Outstanding Research Performance twice, the Faculty Research Grant Achievement Award twice, the Faculty Best Researcher Award, and several teaching awards. He serves and has served as an Editor-in-Chief for the IEEE TRANSACTIONS ON CIRCUITS AND SYSTEMS II (2016–2019), the *IEEE Circuits and Systems Magazine* (2012–2015), an Editor-in-Chief of the *IEEE Circuits and Systems Society Newsletter* (since 2007), an Associate Editor for three IEEE Journal/Transactions, Editor for the *International Journal of Circuit Theory and Applications*, and is on the editorial boards of a few other journals. He currently chairs the steering committee for the IEEE TRANSACTIONS ON NETWORK SCIENCE AND ENGINEERING. He also serves as panel member of the Hong Kong Research Grants Council, and member of several professional and government committees.